Journal of Nanoparticle Research (2007) 9:71–83
DOI 10.1007/s11051-006-9152-z

Special focus: Nanoparticles and Occupational Health

An axial flow cyclone to remove nanoparticles at low pressure conditions

Sheng-Chieh Chen and Chuen-Jinn Tsai
Institute of Environmental Engineering, National Chiao Tung University, Hsin Chu, 300, Taiwan; (E-mail: cjtsai@mail.nctu.edu.tw)

Received 25 July 2006; accepted in revised form 28 July 2006

Key words: axial flow cyclone, nanoparticle control, particle loading effect, particle control equipment, occupational health

Abstract

In this study, the axial flow cyclone used in Tsai et al. (2004) was further tested for the collection efficiency of both solid (NaCl) and liquid (OA, oleic acid) nanoparticles. The results showed that the smallest cutoff aerodynamic diameters achieved for OA and NaCl nanoparticles were 21.7 nm (cyclone inlet pressure: 4.3 Torr, flow rate: 0.351 slpm) and 21.2 nm (5.4 Torr, 0.454 slpm), respectively. The collection efficiencies for NaCl and OA particles were close to each other for the aerodynamic diameter ranging from 25 to 180 nm indicating there was almost no solid particle bounce in the cyclone. The 3-D numerical simulation was conducted to calculate the flow field in the cyclone and the flow was found to be nearly paraboloid. Numerical simulation of the particle collection efficiency based on the paraboloid flow assumption showed that the collection efficiency was in good agreement with the experimental data with less than 15% of error. A semi-empirical equation for predicting the cutoff aerodynamic diameter at different inlet pressures and flow rates was also obtained. The semi-empirical equation is able to predict the cutoff aerodynamic diameter accurately within 9% of error. From the empirical cutoff aerodynamic diameter, a semi-empirical square root of the cutoff Stokes number, $\sqrt{St_{50}^{*}}$, was calculated and found to be a constant value of 0.241. This value is useful to the design of the cyclone operating in vacuum to remove nanoparticles.

Introduction

Cyclones are normally used to remove particles larger than 5–10 μm in aerodynamic diameter. To reduce the cutoff diameter, the cyclone diameter must be reduced or the flow rate must be increased. For example, Zhu and Lee (1999) tested a small tangential cyclone (cyclone diameter, $D = 3.05$ cm) and found the cutoff size to be 0.3 μm when it was operated at 110 slpm (standard L/min). Making use of large slip correction factor of nanoparticles at reduced pressure, Tsai et al. (2004) designed and tested an axial flow cyclone to remove nanoparticles smaller than 100 nm at low pressure conditions. The smallest cutoff aerodynamic diameter in the study is 43.3 nm when the inlet pressure of the cyclone is 6 Torr at the flow rate of 0.455 slpm. However, the experimental results of the collection efficiency are for liquid particles only. The solid particles collection efficiency of the cyclone has not been investigated.

Maynard (2000) is the first to study the particle penetration of the axial flow cyclone in ambient pressure theoretically. He proposed an implicit equation of the particle penetration based on the assumption that particle collection mainly occurs in the vane and body sections. The equation predicts the cutoff aerodynamic very well. Tsai et al. (2004) derived a theoretical equation for the particle collection efficiency based on the air

volumetric flow rate, the geometry of the cyclone, the properties of carrying gas and the pressure of the cyclone. The cutoff aerodynamic diameter D_{pa50} for the cyclone with one vane making three turns was derived as

$$D_{pa50} = \frac{0.106\mu(B-w)\left(r_{max}^2 - r_{min}^2\right)^2}{\rho_{p0}\lambda_0 r_{min}^2 Q_0} \times \left(\frac{P_{cyc}}{P_{760}}\right)^2. \quad (1)$$

In the above equation, μ is the fluid dynamic viscosity (N s/m^2), B is the pitch of vanes (m), w is the vane thickness (m), r_{max} is the inner radius of the cyclone (m), r_{min} is the radius of the vane spindle (m), ρ_{p0} is unit density (1000 kg/m^3), λ_0 is the mean free path of air molecules at standard condition (m), Q_0 is standard volumetric flow rate (m^3/sec), P_{cyc} is the average pressure of cyclone inlet and outlet (Torr), P_{760} is 760 Torr. The equation agrees well with the published experimental data on cutoff diameter (Liu & Rubow, 1984; Weiss et al., 1987; Vaughan, 1988) in ambient conditions. But at low pressure conditions (several Torrs), the equation predicts the cutoff diameter much smaller than the experimental data. The theoretical cutoff diameter has to be adjusted to fit the experimental data. The reason why there is such as discrepancy has yet to be found.

Hsu et al. (2005) derived a model considering both centrifugal and diffusional forces for nanoparticle removal in vacuum using the axial flow cyclone of Tsai et al. (2004). They found that diffusional mechanism was important when particles were smaller than 40 nm.

For impactors, it is well-known that the collection of liquid particles is better than that of solid particles due to solid particles bounce or reentrainment from the impactor substrates (Biswas & Flagan, 1988; Tsai & Cheng, 1995; Tsai & Lin, 2000). Zhu and Lee (1999) studied the differences in the collection efficiency of a tangential flow cyclone for solid and liquid particles. Liquid dioctyl-phthalate (DOP) and solid polystyrene latex (PSL) particles in the size range of 1.0 and 3.6 μm were found to have similar collection efficiencies even at a high flow rate of 80 slpm. However, the effect of solid particle bounce on the collection efficiency of the axial flow cyclone operating in low pressure conditions remains to be investigated.

The effect of deposited solid particles on the cyclone wall of the tangential flow cyclone has been investigated in Blachman and Lippmann (1974) and Tsai et al. (1999). The particle collection efficiency was found to increase with increasing particle mass deposited in the cyclone (Blachman & Lippmann, 1974). Such increase is mainly due to the accumulation of dust on the cyclone wall opposite to the inlet which gradually reduces the effective diameter of the cyclone. But when the amount of deposited particles is heavy enough, the aggregated particles will be detached and then the collection efficiency will reduce again (Blachman & Lippmann, 1974). The effect of different amounts of deposited particle mass on the collection efficiency was not studied in Blachman and Lippmann (1974). The solid particle loading effect on the collection efficiency for a 10 mm nylon cyclone and a new 18 mm aluminum cyclone was studied by Tsai et al. (1999). They found the cutoff aerodynamic diameter of both cyclones decreased with increasing deposited particle mass. But the 18 mm cyclone appeared to have less deposited particle mass effect on the collection efficiency due to its larger inner diameter. The cyclones tested in Blachman and Lippmann (1974) and Tsai et al. (1999) were tangential flow cyclones. There have been no studies on the solid particle loading effect on the collection efficiency for axial flow cyclones.

The flow field in the cyclone is complicated. Several researchers have studied the flow fields numerically for tangential flow cyclones and examined the influence of different geometries and operating conditions on the collection efficiency of the cyclones (Boysan et al., 1983; Hoekstra et al., 1999; Schmidt & Thiele, 2002; Harwood & Slack, 2002; Schmidt et al., 2003; Xiang & Lee, 2004). However, there have been no numerical studies on the flow field and particle collection efficiency of axial flow cyclones, in particular at low pressure conditions.

In this study, NaCl and OA monodisperse nanoparticles in diameter from 12 to 100 nm were generated to test the axial flow cyclone of Tsai et al. (2004). The test conditions are: inlet pressure of 4.3 Torr at 0.351 slpm, 5.4 or 6.0 Torr at 0.455 slpm, and 6.8 or 7.0 Torr at 0.566 slpm.

The 3-D numerical simulation was also conducted in this study to calculate the flow and pressure fields of the cyclone in order to obtain a more accurate prediction of the collection efficiency and cutoff size of the cyclone.

Finally, a new empirical equation for predicting the cutoff aerodynamic diameter of the cyclone was also proposed based on the better knowledge of the 3-D flow and pressure fields obtained in this study.

Experimental

The experimental system is shown in Figure 1. Monodisperse OA (ρ_p = 894 kg/m^3) and NaCl (ρ_p = 2200 kg/m^3) particles in diameter between 12 and 100 nm were generated by the atomization and electrostatic classification technique. Polydisperse particles were first generated by atomizing (Atomizer, TSI Model 3076) 0.05 or 0.1% (v/v) OA and NaCl solution. Then the aerosol flow was dried by a silica gel drier. The dried aerosol stream was passed through a furnace (Lindberg/Blue Model CC58114C-1) and mixed with clean air to produce sufficiently small particles (< 100 nm) after the furnace. The temperature of the furnace was fixed at 650 and 1150 K for OA and NaCl particles, respectively. Fine polydisperse particles were generated by mixing the vapor with dry compressed air. Monodisperse, singly charged particles were generated by classifying the polydisperse particles by a nano-DMA (TSI Model 3085).

The SMPS (Condensation Particle Counter, TSI Model 3022 and Electrostatic Classifier, TSI Model 3071) was used to monitor the concentrations of particles in the monodisperse particle stream from the nano-DMA. The concentrations were used to correct for the multiple charge effect on the collection efficiency. For the detailed procedure, refer to Tsai et al. (2004).

An aerosol electrometer (TSI Model 3068) was used to measure the electric current of the upstream and downstream aerosol concentrations of the cyclone. A homemade Faraday cage with a larger inlet and outlet than the TSI Model 3068 electrometer was used to reduce the pressure drop through it. A critical orifice (O'Keefe Controls

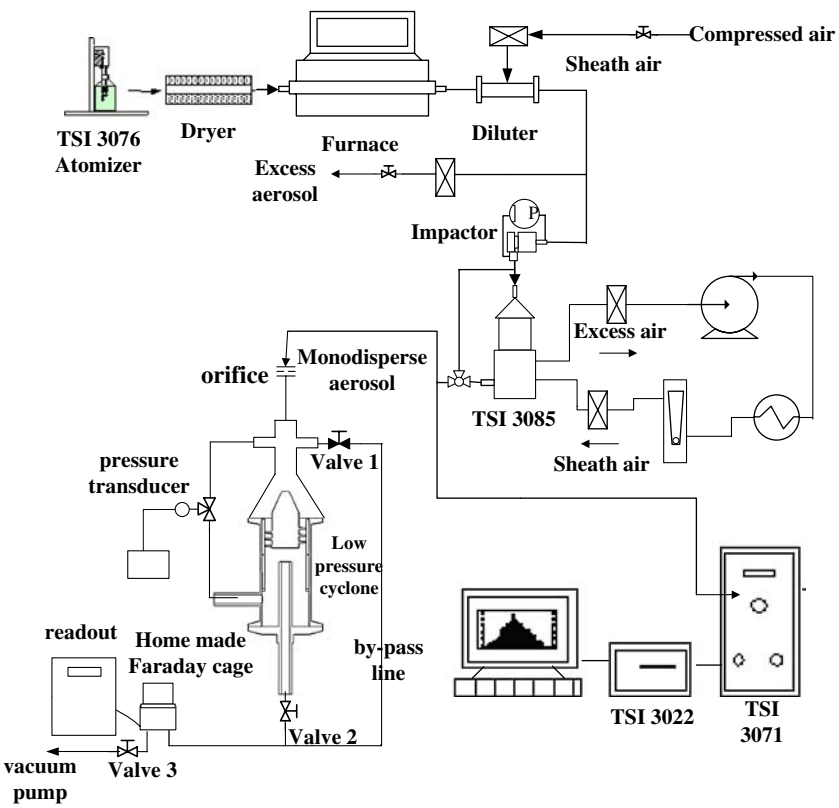

Figure 1. Experimental setup of the present study.

Co., E-8, 0.351 slpm or E-9, 0.455 slpm or E-10, 0.566 slpm) was installed at the cyclone inlet to achieve the low-pressure condition. A powerful vacuum pump (DUO 65, Pfeifeer, Germany, nominal pumping speed: 70 m^3/h) was used to achieve the desired low pressure condition. The inlet pressures at the cyclone inlet in this study are 4.3, 6.0 5.4, 6.8 and 7 Torr.

The bypass line was used to determine the particle concentration at the cyclone inlet which can be controlled by an on-off valve (Valve 1) as shown in Figure 1. When Valve 1 is open and Valve 2 is closed, the aerosol flow will pass through the bypass line and the inlet aerosol concentration can be measured. On the other hand, when Valve 1 is closed and Valve 2 is open, the aerosol flow will pass through the cyclone and the particle concentration at the cyclone outlet can be obtained. By adjusting the angle valve (Valve 3) at the downstream of the Faraday cage, the pressure at the cyclone inlet can be controlled.

The loading effect test was conducted by introducing polydisperse particles continuously into the cyclone over a period of time. The particle collection efficiency was tested after loading polydisperse particles (total number conc.: 8.26×10^6–1.2×10^7#/cm^3, NMD: 69.5–82 nm, σ_g: 1.53–1.58) for 1-h (loaded mass: 0.33 mg), 3-h (1.24 mg), and 5-h (1.73 mg), respectively.

The spindle and vane of the cyclone are shown in Figure 2. The radius of the spindle and the inner radius of the cyclone are 10 and 15 mm, respectively. The width and the height of the vane section are 5 and 4 mm, respectively.

Numerical

Flow field

In order to obtain accurate pressure distribution and gas velocity fields in the cyclone, 3-D numerical simulation was conducted in the present study. The governing equations are Navier–Stokes and the continuity equations. Since the maximum Kundsen number in the present study for the pressure of 1.46 Torr (P_{in} = 4.31 Torr) is around 0.01, the flow was considered as continuum. The maximum Kundsen number, *Kn*,max is calculated as

$$Kn, \max = \frac{2\lambda}{D_o}, \tag{2}$$

where D_o is the inner diameter of the outlet tube (m); λ is the mean free path of the air molecular (m). Moreover, Steady-state and compressible laminar flow was assumed in this study. The Navier–Stokes and the continuity equations were solved by using the STAR-CD 3.15 code (CD-adapco Japan Co., LTD) based on the finite volume discretization method. The pressure-velocity linkage was solved by the SIMPLE (semi-implicit method for pressure linked equation) algorithm (Pantankar, 1980) and the differencing schemes for the space discretization method were the UD (upwind differencing) and CD (central differencing) schemes for the flow velocity and density, respectively.

Multi-block, hybrid (both Hexa. and Tetra.) cells were generated by an automatic mesh generation tool, Pro-Modeler 2003 (CD-adapco Japan Co., LTD). The total number of cells used was about 1,000,000. The average cell length was around 0.5 mm and the smallest length of 0.1 mm was assigned near the surface of the vane.

The convergence criterion of the flow field calculation was set to be 0.01 % for the summation of the residuals. The total number of iterations was about 300 and the time required to reach convergence was about 600 min. Non-slip condition was applied on the walls. A constant mass flow rate (0.351, 0.455, or 0.566 slpm) was set on the inlet boundary assuming uniform velocity profile. On the outlet boundary, a fixed pressure was assigned based to the experimental data.

Particle collection efficiency

As a particle enters the cyclone, it experiences the centrifugal force and migrates toward the wall. The Stokes law was adopted to calculate the particle drag force since the *Rep* (particle Reynolds number) was much small than 0.1 in this study. Based on the assumption that particle drag force is equal to the centrifugal force, the particle radial migration velocity, V_r, is calculated as

$$V_r = \frac{\tau V_t^2}{r}, \tag{3}$$

where V_t is the tangential flow velocity, r is the radial position of the particle and τ is the

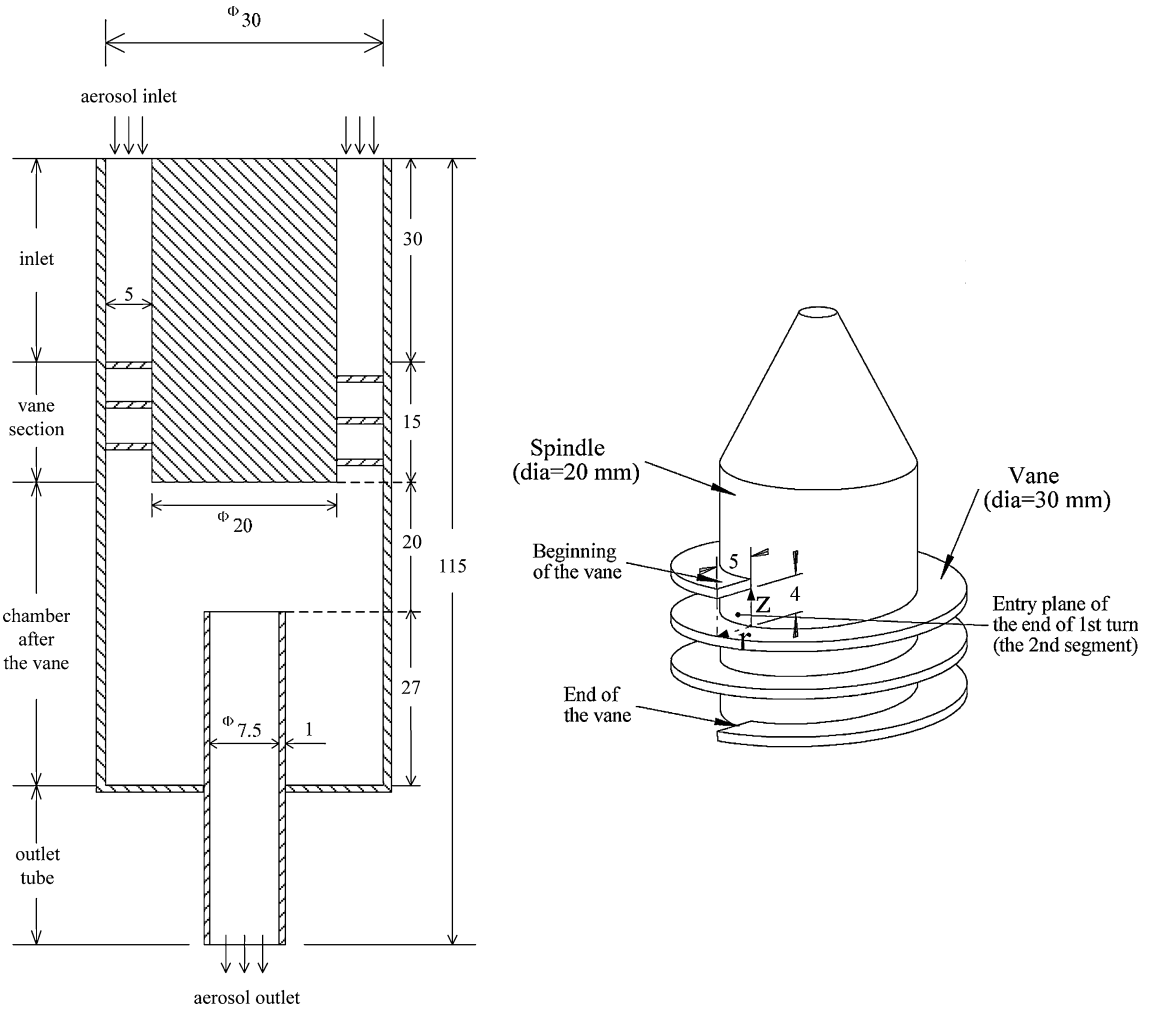

Figure 2. Schematic diagram of the spindle and vane. (the r–z coordinate and the dimension of the vane section are also indicated.)

particle relaxation time, which can be written as

$$\tau = \frac{\rho_{p0} D_{\mathrm{pa}}^2 C(D_{\mathrm{pa}})}{18\mu}, \tag{4}$$

where D_{pa} and $C(D_{\mathrm{pa}})$ are the particle aerodynamic diameter and the slip correction factor, respectively. Both τ and V_{t} are the function of pressure in the cyclone.

The differential radial migration distance of the particle, dr, can be calculated as

$$\mathrm{dr} = V_r dt = \frac{\tau V_t^2}{r} \frac{r \mathrm{d}\theta}{V_t} = \tau V_t \mathrm{d}\theta, \tag{5}$$

The paraboloid flow was assumed to calculate the particle migration distance. Since the flow in the cyclone was found to spin for slightly greater than 2 turns starting slightly ahead of the end of the first turn and ending slightly beyond the end of the third turn, only the particle migration distance during 2 turns was calculated. To simplify the calculation, the total radial migration distance of a particle, Δr, was calculated based on Eq. (5) as the sum of the migration distance from ten segments of the vane section, each segment corresponded to 1/4 turn of the vane. The first segment or the first 1/4 turn was added before the end of the first turn while another 1/4 turn was added after the end of

the third turn. The second and third turn each constituted four segments in the calculation. All together there were 10 segments.

As will be shown later, the tangential flow develops very fast and becomes nearly fully developed near the end of the first turn of the vane. The fully developed profile is paraboloid which can be written as

$$V_{\mathrm{t},n^{\mathrm{th}}}(r,z) = 2(\overline{V}_{\mathrm{t},n^{\mathrm{th}}} - 1)\left[1 - \left(\frac{2z}{4}\right)^2\right] \times \left[1 - \left(\frac{2r}{5}\right)^2\right] + 2, \quad \mathrm{m/s} \tag{6}$$

where the coordinates r and z are illustrated in Figure 2. $V_{\mathrm{t},n^{\mathrm{th}}}(r,z)$ and $\overline{V}_{\mathrm{t},n^{\mathrm{th}}}$ are the tangential velocity of the entry plane of the n^{th} segment at position (r, z) and the average tangential velocity of the n^{th} segment, respectively. The constant 2 m/s at the right-hand side of Eq. (6) represents the tangential velocity near the wall, which is obtained from the numerical simulation shown later. If the total migration distance of a particle of aerodynamic diameter D_{pa} plus the initial radial position is greater than 5 mm (or $r_{\max}$–$r_{\min}$, the width of the vane section) then the particle hits the wall and is collected. Assuming different initial radial positions of a particle at the entry plane of the first segment, the critical curve which delineates the collection and non-collection regions of the particle can be found. As the collection area is obtained, then the collection efficiency can be calculated by the following equation as

$$\eta_{\mathrm{dpa}} = \frac{A_{\times}\overline{V}'_{\mathrm{t},1}}{5 \times 4 \times \overline{V}_{\mathrm{t},1}}, \tag{7}$$

where A is the collection area (mm^2); $\overline{V}'_{\mathrm{t},1}$ is the average tangential velocity of the collection area (m/s); 5 (mm) and 4(mm) are the width and gap of the vane section, respectively (mm); $\overline{V}_{\mathrm{t},1}$ is the average tangential velocity at the entry plane of the 1st segment of the vane section.

Since the pressure drop of the cyclone occurs mainly in the vane section, $\overline{V}_{\mathrm{th},n^{\mathrm{th}}}$ is calculated based on the pressure at the n^{th} section following the ideal gas law and mass conservation principle. For comparison purpose, if the tangential flow field is assumed to be plug flow, the total radial migration distance Δr can be calculated as (referring to Eq. (5))

$$\Delta r = \sum_{n^{\mathrm{th}}=1}^{10} \frac{\pi}{2}\overline{\tau}_{n^{\mathrm{th}}}\overline{V}_{\mathrm{t},n^{th}}, \tag{8}$$

where $V_{\mathrm{t},n^{th}}$ is the average tangential velocity (m/s), $\overline{\tau}_{n^{\mathrm{th}}}$ is the average relaxation time of the particle. Both $V_{\mathrm{t},n^{th}}$ and $\overline{\tau}_{n^{\mathrm{th}}}$ depend on the average pressure at the n^{th} segment. The collection efficiency η of the particle can be calculated as

$$\eta = \frac{\Delta r}{r_{\max} - r_{\min}}. \tag{9}$$

Results and discussion

Comparison of collection efficiency for liquid and solid particles

The collection efficiencies of solid NaCl and liquid OA particles for the inlet pressure of 6 and 5.4 Torr and the sampling flow rate of 0.455 lpm are compared in Figure 3. For OA particles, the present experimental data are in good agreement with Tsai et al. (2004). The collection efficiencies are seen to be greatly improved for both OA and

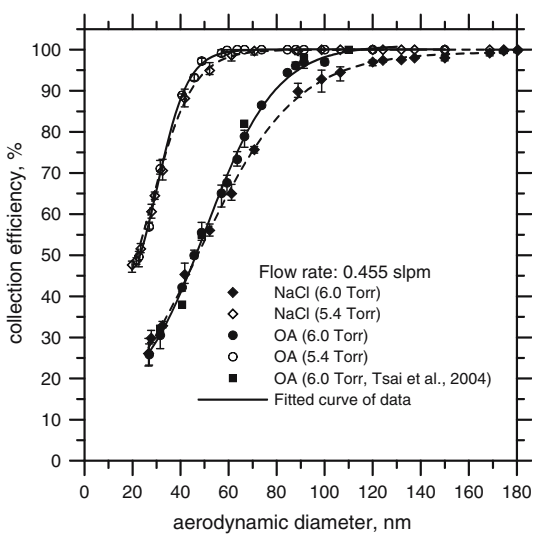

Figure 3. Collection efficiency *versus* particle aerodynamic diameter for solid NaCl and liquid OA particles at different inlet pressures.

NaCl particles when the pressures at the cyclone inlet are reduced from 6 to 5.4 Torr. The cutoff aerodynamic diameters of OA and NaCl particles are reduced from 49.8 and 47.1 to 23.1 and 21.2 nm, respectively as the pressure at the cyclone inlet is decreased from 6 to 5.4 Torr, respectively. In addition, Figure 3 indicates that the collection efficiencies of liquid and solid particles are close to each other for both operation pressures except in the size range from 60 to 120 nm at 6 Torr where the collection efficiency of OA is slightly better (within 10%) than NaCl. This is to say that the effect of solid particle bounce on the collection efficiency is not very obvious. Furthermore, it also found the diffusion effect on collection efficiency for particles less than (40 nm) is not as significant as claimed by Hsu et al. (2005).

Solid particle loading effect on collection efficiency

The effect of polydisperse particle loading on the collection efficiency is shown in Figure 4 for the inlet pressure of 6 and 5.4 Torr, respectively. For both operating pressures, the collection efficiency after 1-h loading (loaded mass: 0.33 mg) is 5–10 % higher than that of a clean cyclone (or zero particle loading). However, the collection efficiency after 3-h (1.24 mg), and 5-h (1.73 mg) loading is not too much different from that of 1-h loading.

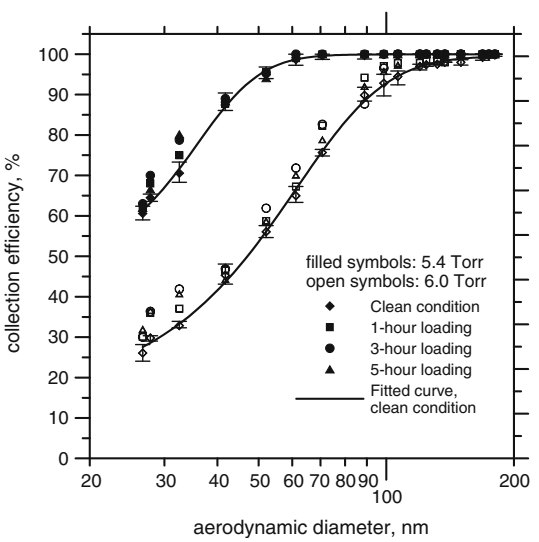

Figure 4. Particle loading effect on collection efficiency, solid NaCl particles.

Tsai et al. (1999) used two monodisperse particles, 3.76 and 6.7 μm in aerodynamic diameter, to examine the solid loading effect on the collection efficiency of a 10 mm nylon cyclone. Both loaded particle masses in the cyclone were 0.06 mg. Their experimental results indicated that the particle penetration decreased (or collection efficiency increased) for both loading conditions compared to that of the clean condition. The present results also show that the collection efficiency increases after particles are loaded in the cyclone. However, the increase in the collection efficiency is larger in Tsai et al. (1999) (10–30 % increases, small 10 mm tangential flow cyclone) than the present study (5–10 % increases, axial flow cyclone). This is due to the accumulation of deposited particles on the cyclone wall opposite to the inlet for the small tangential flow cyclone, which has a larger influence on the collection efficiency. In comparison, the present axial flow cyclone has a larger cyclone diameter and a more uniform particle deposit on the cyclone wall. As a result, the solid particle loading effect on the collection efficiency is not as significant as that of the small tangential flow cyclone.

The collection efficiency of liquid OA particles at 5 different inlet pressures is shown in Figure 5. The flow rate and the Reynolds number range from 0.351 to 0.566 slpm and 4.9 to 8.0, respectively. The Reynolds number, *Re*, is defined as

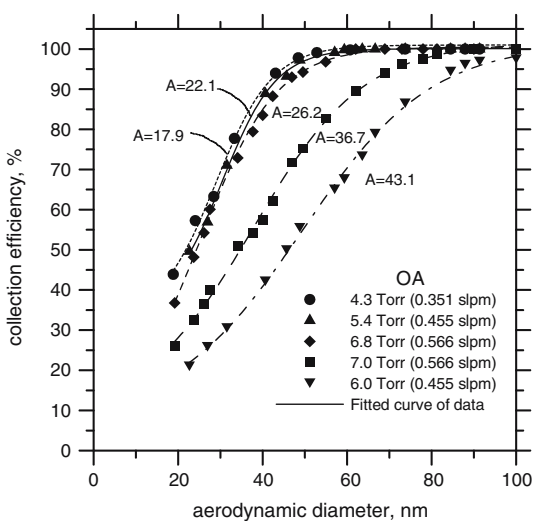

Figure 5. Collection efficiency *versus* particle aerodynamic diameter for OA particles at different inlet pressures and flow rates. (parameter $A = P_{in} \times P_{out}/Q_0$).

$$Re = \frac{\rho(r_{\max} - r_{\min})\overline{V}_a}{\mu}, \qquad (10)$$

where $\rho, \overline{V}_a$ are the gas density (kg/m^3) and the average axial velocity (m/s), respectively. $\rho, \overline{V}_a$, and μ were evaluated at the entry of the vane section. The figure shows that the parameter A, which is defined as $A = P_{\text{in}} \times P_{\text{out}}/Q_0$ (P_{in}: pressure at the cyclone inlet; P_{out}: pressure at the vane outlet), influences the collection efficiency and cutoff diameter. The larger A is the smaller collection efficiency the cyclone becomes. The cutoff size is 21.7, 23.1, 25.6 nm for the inlet pressure of 4.3 Torr at 0.351 slpm (A = 17.93), 5.4 Torr at 0.455 slpm (A = 22.08), and 6.8 Torr at 0.566 slpm (A = 26.19) (also shown in Table 1). The cutoff size becomes much larger for the inlet pressure of 7.0 Torr at 0.566 slpm (A = 36.73), 6.0 Torr at 0.455 slpm (A = 43.12) as the parameter A becomes much larger for these two cases (also shown in Table 1). The reasons why the cutoff size is affected by A will be explained later when the empirical equation for cutoff size is derived.

Numerical results for flow field and particle collection efficiency

The simulated results for the pressure distribution and the maximum tangential velocity in the vane section for P_{in} = 5.4 Torr (0.455 slpm) are shown in Figure 6. It can be seen that the tangential velocity remains small in the beginning of the first turn of the vane. However, it increases sharply from the entry plane of the first segment (or the beginning of 3/4 turn). Then it increases exponentially until the end of 3 turns (or the ninth segment) and reduces sharply in the tenth segment.

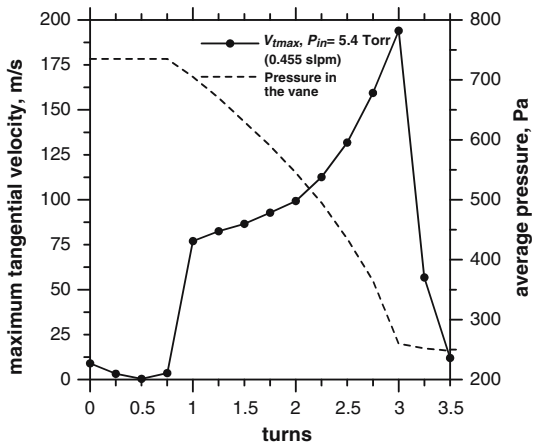

Figure 6. Maximum tangential velocity and pressure distribution in the vane, numerical results.

The tangential velocity peaks at 187 m/s at the end of 3 turns and is reduced to 60 m/s sharply at the end of 10th segment.

The pressure distribution shown in Figure 6 corresponds well with the tangential velocity distribution. The flow is accelerated in the tangential direction as the pressure is decreased in the vane. The pressure remains at about 735 Pa (5.5 Torr, within 2% of the experimental data) in the first turn and then drops monotonically in the second and third turns. Finally, the pressure remains nearly constant at 260 Pa (1.95 Torr) after the end of the third turn. That is, the pressure drop occurs almost entirely in the second and third turns. The figure shows that the flow does not make three full turns as the vane does. Rather, it makes slightly more than two turns only. This is one of the main reasons why the differences are large between the experimental cutoff aerodynamic diameters and the theoretical values in Tsai et al. (2004) in which

Table 1. Cutoff aerodynamic diameter at different operating conditions, liquid oleic acid (OA) particles

Q_0 (slpm)	0.351 Re = 4.9	0.455 Re = 6.4	0.566 Re = 8.0	0.566 Re = 8.0	0.455 Re = 6.4
p_{in} (Torr)	4.31	5.43	6.77	7.00	6.00
p_{out}(Torr)	1.46	1.85	2.19	2.97	3.27
$A = P_{in} \times P_{out}/Q_0$	17.93	22.08	26.19	36.73	43.12
Exp. D_{pa50}(nm)	21.69	23.14	25.58	34.71	46.25
Num_{parab} D_{pa50}(nm)	20.4	23.3	25.21	31.2	39.8
Num_{plug} D_{pa50}(nm)	18.1	20.2	23.6	30.6	34.3
Theo. D_{pa50} (nm), Eq. (8)	13.2	16.5	19.3	27.1	31.8
K (Exp./Theo.)	1.64	1.4	1.33	1.28	1.45

the tangential flow was assumed to make three full turns and the tangential velocity was assumed to be plug flow.

Figure 7 a, b show the tangential velocity profile at the vertical cut planes at the end of 2 and 3 turns, respectively. The tangential velocity peaks near the center of the plane in both figures and the value is about two times the average tangential velocity, which was given in Tsai et al. (2004) as

$$\overline{V_t} = \frac{2r_{min}Q}{(r_{max}^2 - r_{min}^2)(B-w)}, \tag{11}$$

where Q is the volumetric flow rate and can be calculated as

$$Q = Q_0 \frac{P_{760}}{\sqrt{P_{in}P_{out}}}. \tag{12}$$

It is also found that the velocity near the wall is not zero but about 2 m/s. Similar results can be found in other cut planes and at other different operating conditions (P_{in} = 4.3, 6, 6.8 and 7 Torr). From the simulated tangential velocity shown in Figure 7a and b, the velocity profile is found to be nearly paraboloid, and the variation of velocity with r and z positions can be calculated by Eq. (6).

Figure 8a shows the critical collection curves for a 23 nm particle passing through the full three

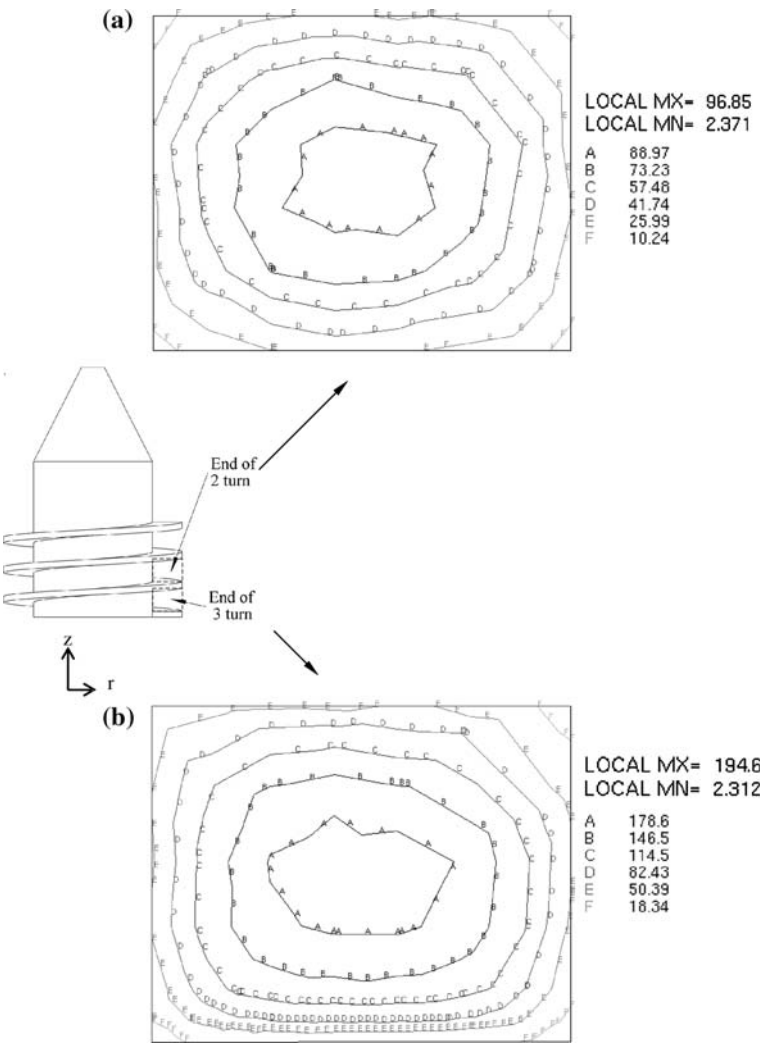

Figure 7. Tangential velocity profile at the cut plane of the vane section, the end of (a) two turns and (b) three turns.

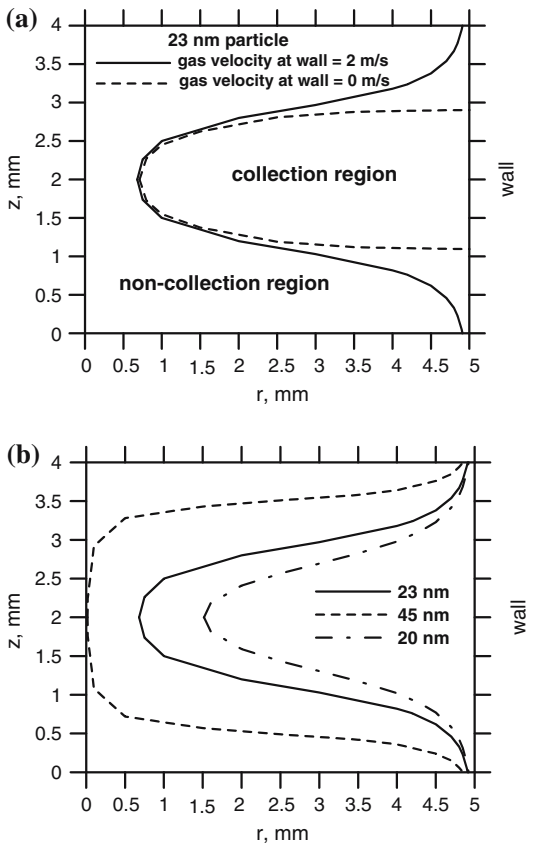

Figure 8. Critical curves at the entry plane of the first segment for particle collection. (a) With or without a constant tangential velocity of 2 m/s at the wall for a 23 nm particle. (b) With a constant tangential velocity of 2 m/s at the wall for 20, 23, and 45 nm particles.

turns of the vane with and without considering the tangential velocity of 2 m/s near the wall, respectively. The area to the right hand side of curve is the particle collection region in which a 23 nm particle will be collected in the cyclone when it starts from this region at the entry of the vane section. Otherwise, it won't be collected. Considering the tangential velocity of 2 m/s on the wall results in a 7% increase in the collection area, and a similar increase in the collection efficiency. The collection areas of three different particle sizes, 20, 23, and 45 nm, are shown in Figure 8b. It shows larger particles have larger collection area than small particles and hence the collection efficiency is also larger.

The experimental particle collection efficiencies and numerical results based on the plug or paraboloid flow assumptions are shown in Figure 9. For the operating conditions at P_{in} = 4.3, 5.4, and 6.8 Torr (Figure 9a), and P_{in} = 6 and 7 Torr (Figure 9b). Figure 9a shows that both numerical results agree with the experimental collection efficiencies very well, especially near the cutoff aerodynamic diameter. The error in the numerical prediction of the cutoff aerodynamic diameter by the paraboloid flow assumption is 5.9, 0.7, and 1.5%, for P_{in} = 4.3, 5.4, and 6.8 Torr, respectively. In comparison, the error by the plug flow assumption is larger, which is 16.6, 12.8, and 7.7%,

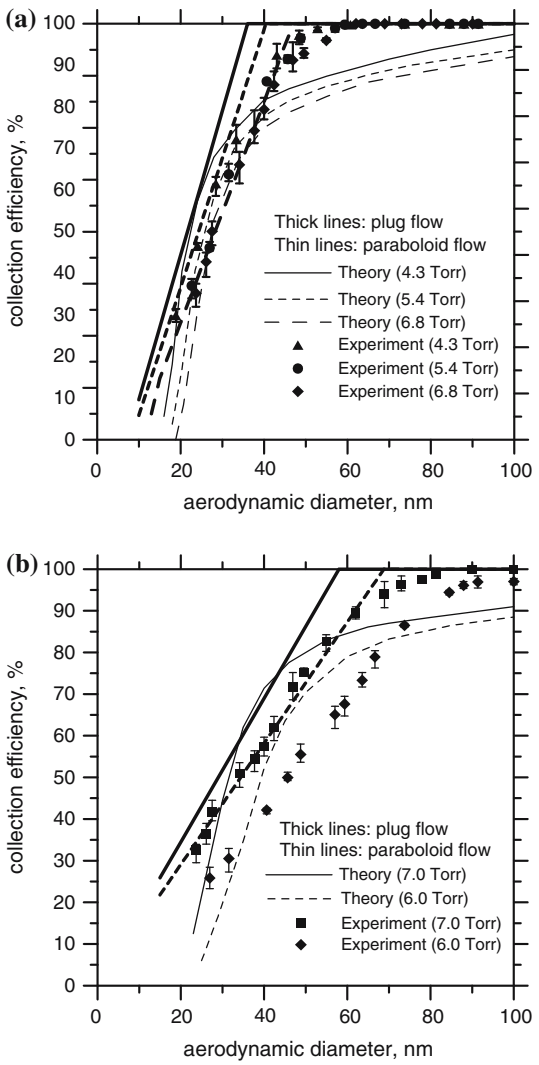

Figure 9. Comparison of numerical collection efficiencis and experimental data. (a) P_{in} = 4.3, 5.4, and 6.8 Torr. (b) P_{in} = 6 and 7 Torr.

for P_{in} = 4.3, 5.4, and 6.8 Torr, respectively. The plug flow assumption over-estimates while the paraboloid flow assumption under-estimates the collection efficiencies when the particle diameter is greater than the cutoff aerodynamic diameter. The maximum difference for the paraboloid flow assumption is around 12%, which is slightly better than the plug flow assumption of 15%.

In Figure 9b, it is seen larger differences occur between the experimental data and theories than in Figure 9a. The error of the cutoff aerodynamic diameter by the paraboloid flow assumptions is 13.9 and 10.1% for P_{in} = 6 and 7 Torr, respectively. In comparison, the error of the plug flow assumption is 25.8 and 11.8 % for P_{in} = 6 and 7 Torr, respectively. The paraboloid assumption predicts the cutoff diameter better than the plug flow assumption.

The differences between the numerical results and the experimental data are mainly due to the over-simplified assumption of either plug flow or paraboloid flow. In fact, the flow is developing near the entry of the vane section. Errors may also be caused by the assumption of a constant velocity of 2 m/s near the wall. In addition, calculating the total migration distance Δr from summing the migration distances of ten segments may also induce errors.

Although the present method is good in predicting the cutoff diameter and collection efficiency, it is not possible to obtain an analytical equation to calculate the cutoff diameter. The following section describes a modified empirical method from Tsai et al. (2004), which can be used to predict the cutoff aerodynamic based on the inlet pressure, flow rate, and cyclone dimension.

Semi-empirical equation for cutoff aerodynamic diameter

In this study, the theoretical derivation of the particle collection efficiency is similar to our previous study (Tsai et al., 2004) but the pressure drop through the vane section is assumed to be linear. The pressure at n^{th} turn of the vane can be defined based on P_{in} (pressure at the cyclone inlet) and P_{out} (pressure at the vane outlet) as

$$P_n = P_{in} - n \times \frac{P_{in} - P_{out}}{n_T}, \tag{13}$$

where the n_T is the total number of turns of the vane and is fixed to 2 based on the present numerical results. The volumetric flow rate and particle relaxation time will change in the vane section with respect to pressure. The plug flow assumption was used to facilitate the derivation of the theoretical collection efficiency, which is known to under-predict the cutoff diameter. By comparing the experimental cutoff diameters with the theoretical values, we can obtain an empirical factor K to adjust the theoretical values.

Integrating the particle radial velocity and the residence time in the two complete turns, the particle total migration distance (Δr) in the vane section is obtained. The particle collection efficiency is then calculated as in Eq. (9). By setting η = 0.5 in Eq. (9), the theoretical cutoff aerodynamic diameter, $D_{pa50,theo}$, can be derived as

$$D_{pa50,theo} = \frac{0.11\mu(B-w)\left(r_{max}^2 - r_{min}^2\right)(r_{max} - r_{min})}{\rho_{p0}\lambda_0 r_{min} P_{760}^2} \times A, \tag{14}$$

where $A = P_{in} \times P_{out}/Q_0$, which is the important operating parameter of the cyclone as described earlier.

The collection efficiencies of liquid OA particles at 5 different operation conditions are shown in Figure 5 as described in the previous section. The comparison of experimental cutoff diameters at different inlet pressures with the numerical values and the theoretical values by Eq. (14) is shown in Table 1. As expected, the theoretical values are smaller than the experimental results. Therefore, an empirical factor K, which is defined as the ratio of the experimental cutoff size to the theoretical value, is suggested to adjust the theoretical cutoff size. In Table 1, K is shown to be relatively constant with the average and standard deviation of 1.4 and 0.126, respectively. That is, the semi-empirical cutoff aerodynamic diameter can be rewritten as:

$$D_{pa50} = 1.4 D_{pa50,theo} = \frac{0.154\mu(B-w)\left(r_{max}^2 - r_{min}^2\right)(r_{max} - r_{min})}{\rho_{p0}\lambda_0 r_{min} P_{760}^2} \times A. \tag{15}$$

The above semi-empirical equation is easy to use and is able to predict the cutoff aerodynamic diameter accurately within 9% of error.

If the collection efficiencies are plotted against $\sqrt{St/St_{50}}$, all the experimental data of five

different conditions for OA particles are collapsed into a single curve as shown in Figure 10. In the figure, St is defined as

$$St = \frac{\tau \overline{V_t}}{r_{max} - r_{min}} \tag{16}$$

and St_{50} corresponds to St at 50% collection efficiency. Referring to Tsai et al. (2004), the slip correction factor used to calculate the particle relaxation time (see Eq. (4)) is given as

$$C(D_{pa}) = \frac{1.695 P_{760} \lambda_0}{\sqrt{P_{in} P_{out}} D_{pa}/2}. \tag{17}$$

$\sqrt{P_{in} P_{out}}$ is used in this study as the average pressure on which many other parameters depend. Combing Eqs. (4), (11), (12) and (17), St in Eq. (16) is rearranged as

$$St = \frac{0.377 r_{min} \lambda_0 \rho_{p0} P_{760}^2}{\mu (r_{max} - r_{min})(r_{max}^2 - r_{min}^2)(B - w) A} \times D_{pa}. \tag{18}$$

It is observed in Figure 10 that all experimental data of particle collection efficiency almost fall on a unique curve, which can be fitted by the following Boltzmann function as

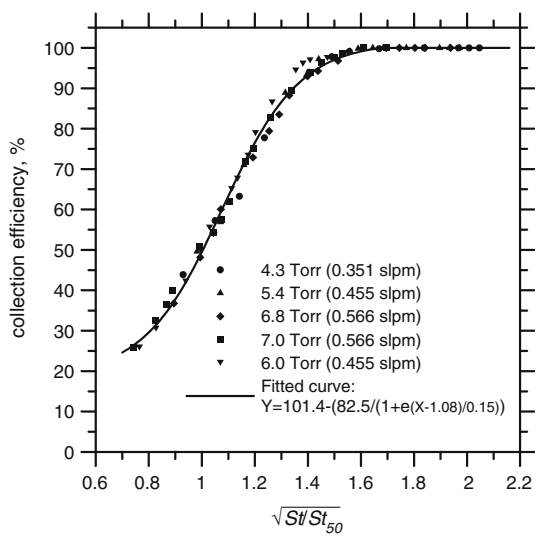

Figure 10. Collection efficiencies *versus* $\sqrt{St/St_{50}}$ for OA particles at different inlet pressures and flow rates.

$$Y = 101.4 - \frac{82.5}{1 + e^{(X-1.08)/0.15}}, X < 1.7, \tag{19}$$

where Y and X are collection efficiency ($\eta(\%)$) and $\sqrt{St/St_{50}}$, respectively.

Replacing D_{pa} in Eq. (18) by the semi-empirical cutoff aerodynamic diameter, D_{pa50} of Eq. (15), the semi-empirical $\sqrt{St_{50}^*}$ can be calculated as

$$\sqrt{St_{50}^*} = \sqrt{\frac{0.377 r_{min} \lambda_0 \rho_{p0} P_{760}^2}{\mu (r_{max} - r_{min})(r_{max}^2 - r_{min}^2)(B - w) A}} \times D_{pa50}. \tag{20}$$

Substituting Eq. (15) into Eq. (20), $\sqrt{St_{50}^*}$ is found to be a fixed value of 0.241. The experimental collection efficiency *versus* $\sqrt{St}$ (calculated from Eq. (18)) for all five test conditions was plotted (not shown here), and the experimental $\sqrt{St_{50}}$ was calculated to be 0.256, 0.240, 0.222, 0.226 and 0.240 for P_{in} = 4.3, 5.4, 6.8, 7.0 and 6.0 Torr, respectively. The difference between the experimental $\sqrt{St_{50}}$ and the semi-empirical $\sqrt{St_{50}^*}$, or 0.241, is −6.2, 0.4, 7.9, 1.5 and 0.4 % for P_{in} = 4.3, 5.4, 6.8, 7.0 and 6.0 Torr, respectively. That is, for the present axial flow cyclone for removing nanoparticles, the design value for the square root of the cutoff Stokes number is

$$\sqrt{St_{50}^*} = 0.241. \tag{21}$$

This value is much smaller than the $\sqrt{St_{50}}$ of the circular jet and rectangular jet impactor, which is 0.49 and 0.77, respectively (Hinds, 1999).

Conclusions

In this study, the axial flow cyclone of Tsai et al. (2004) was further tested for the collection efficiencies of solid NaCl and liquid OA nanoparticles in the diameter from 12 to 100 nm at low-pressure conditions (4.3, 5.4, 6.0, 6.8, and 7.0 Torrs). The objective was to find whether solid particle bounce would influence the collection efficiencies. The axial flow cyclone was shown to be able to remove NaCl and OA nanoparticles below 50 nm efficiently. The smallest cutoff aerodynamic diameters of OA and NaCl particles were found to be 21.7 (4.3 Torr, 0.351 lpm) and 21.2 (5.4 Torr, 0.454 lpm), respectively. Differences in the collection efficiencies of

liquid and solid particles were within 10% indicating that the effect of solid particle bounce on the collection efficiency was not very obvious. The test for the solid particle loading in the cyclone further indicated a soiled cyclone wall did not change the collection efficiency too much ($< 10\%$).

In order to predict the collection efficiency and cutoff diameter accurately, a 3-D numerical simulation was conducted to obtain the pressure distribution and gas velocity fields in the cyclone. Results showed that the tangential flow developed quickly into paraboloid flow profile near the end of the first turn of the vane section. Total migration distance was calculated based on the local tangential flow velocity and pressure to obtain the numerical collection efficiency.

The comparison of the experimental particle collection efficiencies and cutoff diameters with the numerical simulations showed that the Paraboloid tangential flow assumption yielded better results than the plug flow assumption, with the maximum error of 15% for the collection efficiencies and 13.9% for the cutoff diameters, respectively.

Based on the simulated pressure and tangential flow fields, a modified theoretical method from Tsai et al. (2004) was proposed. The semi-empirical equation was then developed to predict the cutoff aerodynamic diameter and the cutoff Stokes number accurately within 9% and 8% of error, respectively. Based on the semi-empirical cutoff aerodynamic diameter, the design value of the square root of the cutoff Stokes number, $\sqrt{St_{50}^{*}}$, was calculated and found to be a constant value of 0.241.

Acknowledgement

Authors would like to thank for the financial support of this project by Taiwan National Science Council (NSC 94-2211-E-009-001).

References

Biswas P. & R.J. Flagan, 1988. Particle trap impactor. Aerosol Sci. 19, 113–121.

Blachman M.W. & M. Lippmann, 1974. Performance characteristics of the multicyclone aerosol sampler. Am. Ind. Hyg. Assoc. J. 35, 311–326.

Boysan F., B.C.R. Ewan, J. Swithenbank & W.H. Ayers, 1983. Experimental and theoretical studies of cyclone aeparator aerodynamics. IChemeE. Symp. Series 69, 305–320.

Harwood R. & M. Slack, 2002. CFD analysis of a cyclone. QNET-CFD Network Newsletter. 1, 25–27.

Hinds W.C., 1999 Aerosol Technology. New York: Wiley 126.

Hoekstra A.J., J.J. Derksen & H.E.A. Van Den Akker, 1999. An experimental and numerical study of turbulent swirling flow in gas cyclones. Chem. Eng. Sci. 54, 2055–2065.

Hsu Y.D., H.M. Chein, T.M. Chen & C.J. Tsai, 2005. Axial flow cyclone for segregation and collection of ultrafine particle: Theoretical and experimental study. Environ. Sci. Technol. 39, 1299–1308.

Liu B.Y.H. & K.L. Rubow, 1984. A new axial flow cascade cyclone for size characterization of airborne particulate matter. In: Liu B.Y.H., Pui D.Y., & Fissan H.J. ed. Aerosols. Elsevier, Amsterdam, pp. 115–118.

Maynard A.D., 2000. A simple model of axial flow cyclone performance under laminar flow conditions. J. Aerosol Sci. 31, 151–167.

Patankar S.V., 1980 Numerical Heat Transfer and Fluid Flow. Washington: Hemisphere Publishing Co.

Schmidt S. & F. Thiele, 2002. Comparison of numerical methods applied to the flow over wall-mounted cubes. Inter. J. Heat & Fluid Flow. 23, 330–339.

Schmidt S., H.M. Blackburn, M. Rudman & I. Sutalo, 2003. Simulation of turbulent flow in a cyclonic separator. 3rd International conference on CFD in the Minerals and Process Industries CSIRO, Melbourne, Australia, 10–12 December 2003, p. 365–369.

Tsai C.J., H.G. Shiau, K.C. Lin & T.S. Shih, 1999. Effect of deposited particles and particle charge on the penetration of small sampling cyclones. J. Aerosol Sci. 30, 313–323.

Tsai C.J. & T.I. Lin, 2000. Particle collection efficiency of different impactor designs. Sep. Sci. Technol. 35, 2639–2650.

Tsai C.J. & Y.H. Cheng, 1995. Solid particle collection characteristics on impaction surfaces of different designs. Aerosol Sci. Technol. 23, 96–106.

Tsai C.J., D.R. Chen, H.M. Chein, S.C. Chen, J.L. Roth, Y.D. Hsu, W. Li & P. Biswas, 2004. Theoretical and experimental study of an axial flow cyclone for fine particle removal in vacuum conditions. J. Aerosol Sci. 35, 1105–1118.

Vaughan N.P., 1988. Construction and testing of an axial flow cyclone pre-separator. J. Aerosol Sci. 19, 295–305.

Weiss Z., P. Martinec & J. Vitek, 1987. Vlastnosti Dulnibo Prachu A Zaklady Protiprasne Techniky. Prague: SNTL.

Xiang R.B. & K.W. Lee, 2004. The flow pattern in cyclones with different cone dimensions and its effect on separation efficiency. Abstract, EAC 2004, Budapest, Hungary, Sep. 6–10, p. 289–290.

Zhu Y. & K.W. Lee, 1999. Experimental study on small cyclones operating at high flowrates. J. Aerosol Sci. 30, 1303–1315.